Structural and Functional Aberrations in the Cerebral Cortex of Tenascin-C Deficient Mice

Andrey Irintchev[1], Astrid Rollenhagen[1,3], Edgardo Troncoso[2,4], Jozsef Z. Kiss[2] and Melitta Schachner[1]

[1]Zentrum für Molekulare Neurobiologie, Universität Hamburg, D-20246 Hamburg, Germany and [2]Department of Morphology, University Medical Center, 1 rue Michel Servet, CH-1211 Geneva 4, Switzerland
[3]Present address: Institute of Anatomy and Cell Biology, Albert-Ludwigs-Universität Freiburg, D-79104 Freiburg, Germany
[4]Present address: Prefargier Psychiatric Hospital, CH-2074 Marin, Neuchatel, Switzerland

The extracellular matrix glycoprotein tenascin-C (TNC) has been implicated in neural development and plasticity but many of its functions *in vivo* remain obscure. Here we addressed the question as to whether the constitutive absence of TNC in mice affects cortical physiology and structure. Defined major cell populations (neurons and inhibitory neuronal subpopulations, astrocytes, oligodendrocytes and microglia) were quantified in the somatosensory and motor cortices of adult TNC deficient (TNC−/−) and wild-type (TNC+/+) mice by immunofluorescence labelling and stereology. In both areas studied we found abnormally high neuronal density, astrogliosis, low density of parvalbumin-positive interneurons and reduced ratios of oligodendrocytes to neurons and of inhibitory to excitatory neurons in the TNC deficient as opposed to the non-deficient animals. Analysis of Golgi-impregnated layer V pyramidal neurons in TNC−/− animals showed aberrant dendrite tortuosity and redistribution of stubby spines within first- to third-order dendritic arbors. Significantly enhanced responses upon whisker stimulation were recorded epicranially over the barrel and the motor cortices of TNC−/− as compared to TNC+/+ animals, and this effect might be associated with the diminished inhibitory circuitry. These results indicate that TNC is essential for normal cortical development and function.

Keywords: cell density, cerebral cortex, immunohistochemistry, somatosensory evoked potentials, tenascin-C deficient mice

Introduction

Tenascin-C (TNC) is an extracellular matrix (ECM) glycoprotein abundantly expressed in neural and non-neural tissues during normal development, repair processes in the adult organism and tumorigenesis (Vollmer, 1994; Faissner and Schachner, 1995; Bartsch, 1996; Jones and Jones, 2000). In the developing central nervous system (CNS) of rodents, TNC is expressed in specific spatial and temporal patterns in different brain regions. As implicated from *in vitro* studies (for a review, see Jones and Jones, 2000), this expression must be of importance during major developmental processes such as cell proliferation, cell migration and axonal guidance, as well as synaptic plasticity in the adult organism, a notion gaining increasing support from studies on mutant mice (Saga *et al.*, 1992; Forsberg *et al.*, 1996; Evers *et al.*, 2002). Altered rates of oligodendrocyte precursor cell proliferation and migration, as well as apoptotic cell frequency, have been found (Garcion *et al.*, 2001). Abnormalities in locomotion and transmitter systems have been reported (Fukamauchi *et al.*, 1996, 1997, 1998; Kiernan *et al.*, 1999). Impairment of synaptic plasticity has been documented in the hippocampus, a brain region characterized by postnatal expression of TNC (Evers *et al.*, 2002). Although the mechanisms causing these phenomena remain to be elucidated, the outlined results clearly indicate that TNC is a physiologically important component of the CNS.

An area of prominent TNC expression in the developing CNS of rodents is the cerebral cortex (Crossin *et al.*, 1989; Steindler *et al.*, 1989, 1990; Mitrovic *et al.*, 1994; Götz *et al.*, 1997, 1998; Stoykova *et al.*, 1997). TNC is expressed from the onset of cortical development in radial glial cells which not only provide scaffolding for migrating neurons but also participate in the generation of both neuronal and glial cells (Doetsch, 2003; Rakic, 2003). As corticogenesis proceeds, TNC appears in the marginal and subplate zones and becomes widely expressed in the postnatal cortex, from where it gradually disappears by the end of the second week. The temporal pattern of protein expression coincides with periods of generation and migration of diverse cortical cells, establishment of synaptic connections, myelination and rapid functional tissue maturation.

To elucidate the importance of TNC for normal cortical development and function, we investigated adult TNC deficient and wild-type control animals. We performed a quantitative immunocytochemical analysis of several major cell types in the motor and somatosensory cortices. The cellular composition of the cortex of TNC–/– mice was found to be abnormal in comparison to non-deficient animals in several aspects. In addition, we observed structural aberrations in cortical pyramidal neurons as identified in Golgi-stained preparations pointing to the importance of TNC in cortical neuron development. Finally, we tested the overall cortical activity by recording evoked potentials over the motor and barrel cortices upon whisker stimulation. Enhanced responses were found in TNC–/– as compared to TNC+/+ animals which may be related to the observed structural abnormalities.

Materials and Methods

Animals

TNC deficient (TNC−/−) and non-deficient (TNC+/+) littermates used in this study were offspring of heterozygous (TNC +/−) parents and had a C57BL/6J-129SvJ genetic background (Evers *et al.*, 2002). The animals were bred at the specific pathogen-free animal facility of the University of Hamburg Medical School. Male animals (n = 8 per genotype) were used for physiological recordings at the age of 3 months. Morphological investigations were performed on tissue sections from adult female animals (19-23 weeks, referred to in the text as 5 months, n = 5 per genotype). Mean body weight of TNC–/– and TNC+/+ animals did not differ (29 ± 3.6 versus 29 ± 3.3 g and 28 ± 2.4 versus 26 ± 2.8 g in mutant and wild-type mice used for physiology and morphology respectively, P > 0.05, Student's *t*-test). For Golgi impregnations, brains of 3 month old male and female animals were used (n = 7 and 8 for TNC+/+ and TNC–/– respectively). In addition to these experimental groups, 10 female C57BL/6J mice (2-6 months old) were used to optimize

the immunohistochemical stainings and the morphological quantification procedures. All treatments were performed in accordance with the German and Swiss laws for protection of experimental animals. For the physiological experiments (recording of evoked potentials, see below), permission has been obtained from the Office Vétérinaire Cantonal of Geneva.

Preparation of Tissue for Morphological Analyses

Mice were anaesthetized with 16% w/v solution of sodium pentobarbital (Narcoren®, Merial, Hallbermoos, Germany, 5 μl/g body weight, i.p.). After surgical tolerance was achieved, the animals were transcardially perfused with physiological saline for 60 s followed by fixative (4% w/v formaldehyde and 0.1% w/v CaCl$_2$ in 0.1 M cacodylate buffer, pH 7.3, 15 min at room temperature, RT). Cacodylate buffer supplemented with calcium was selected to ensure optimal tissue fixation including preservation of highly soluble antigens, such as S-100 (Rickmann and Wolff, 1995a). Following perfusion, the brains were left *in situ* for 2 h at RT to minimize fixation artefacts (Garman, 1990) after which they were dissected out without the olfactory bulbs and post-fixed overnight (18–22 h) at 4°C in the formaldehyde solution used for perfusion supplemented with 15% w/v sucrose. Tissue was then immersed in 15% sucrose solution in 0.1 M cacodylate buffer, pH 7.3, for an additional day at 4°C.

The fixed and cryoprotected (sucrose-infiltrated) brains were placed into a mouse brain matrix (World Precision Instruments, Berlin, Germany) and a cut was performed through the most caudal slot of the matrix (i.e. close to the caudal pole of the cerebellum). Finally, the tissue was frozen in 2-methyl-butane (isopentane) precooled to –30°C in the cryostat for 2 min and stored in liquid nitrogen until sectioned.

For sectioning, the rostral pole of each brain was attached to a cryostat specimen holder using a drop of distilled water placed on a pre-frozen layer of TissueTek® (Sakura Finetek Europe, Zoeterwoude, The Netherlands). The ventral surface of the brain was oriented so as to face the cryostat knife edge and serial coronal sections of 25 μm thickness were cut in a caudal-to-rostral direction on a cryostat (Leica CM3050, Leica Instruments, Nußloch, Germany). Sections from 1 mm tissue thickness (40 × 25 μm) were picked up on a series of 10 SuperFrost®Plus glass slides (Roth, Karlsruhe, Germany) so that four sections 250 μm apart were present on each slide. Nine 10-slide series (360 sections, 9 mm) were obtained from each specimen, i.e. the whole brain was cut except for the rostral cerebral pole. The sections were air-dried for at least 1 h at RT and stored in boxes at –20°C until stainings were performed.

Selection of Markers and Optimization of the Staining Procedure

To ensure quality of the immunofluorescence for quantitative analysis, we studied the effects of different variables (pretreatment of sections, antibody dilution, incubation time, type of secondary antibody, etc.) in a series of pilot investigations using tissue sections from C57BL/6J mice. For some cell types, antibodies raised against different established markers were evaluated, e.g. glial fibrillary acidic protein (GFAP) and S-100 for astrocytes, neuron-specific enolase (NSE), neuron-specific nuclear antigen (NeuN) and neurofilaments for neurons. Three observations are worth mentioning here. First, high-temperature (80°C) antigen retrieval with sodium citrate, pH 9.0, performed in a waterbath (Jiao *et al.*, 1999), significantly enhanced the staining intensity and reduced background levels with all antibodies tested without negative influence on tissue morphology. Second, prolonged incubation (3 days) was required to reach sufficient staining intensity and depth penetration of the primary antibody. The numerical density of oligodendrocytes (see below) estimated in tissue sections after 1, 3 and 5 days of incubation were similar at 3 and 5 days but lower by a factor of two after 1 day. And finally, in our hands, staining for NeuN appeared better suited than that for neurofilaments or NSE for quantitative analysis of neurons in the cortex.

Antibodies

The following commercially available antibodies were used at optimal dilutions: anti-parvalbumin (PV, mouse monoclonal, clone PARV-19, Sigma, Taufkirchen, Germany, dilution 1:1000, 9.8 μg/ml immunoglobulin, Ig), anti-NeuN (mouse monoclonal, clone A60, Chemicon, Hofheim, Germany, 1:1000, 1 μg/ml Ig), anti-cyclic nucleotide phosphodiesterase (CNPase, mouse monoclonal, clone 11–5B, 1:1000, Sigma, 7.5 μg/ml Ig), anti-glutamic acid decarboxylase 65/67 (GAD, Sigma, rabbit polyclonal, purified IgG fraction, 1:500, 24.6 μg/ml IgG), anti-calbindin (CB, Sigma, rabbit polyclonal, affinity purified, 1:1000, 0.5 μg/ml Ig), anti-calretinin (CR, Sigma, rabbit polyclonal, affinity purified, 1:250, 3.2 μg/ml Ig), anti-S-100 (DakoCytomation, Hamburg, Germany, rabbit polyclonal, purified IgG fraction, 1:500, 9 μg/ml IgG) and Iba1 (Wako Chemicals, Neuss, Germany, rabbit polyclonal, affinity purified, 1:1500, 0.3 μg/ml IgG). The rabbit polyclonal antibody KAF 9-2 raised against TNC has been previously described (Bartsch *et al.*, 1994) and was used at a dilution of 1:100. Biotin-conjugated lectin (*Wisteria floribunda* agglutinin, WFA, Sigma, *N*-acetylgalactosamine specificity) was used at dilution of 1:500 to visualize perineuronal nets.

Immunofluorescence Staining

The general protocol, also used in previous work (Irintchev *et al.* 1993, 1994, 1998), is based on a method described by Sofroniew and Schrell (1982) allowing repeated use of antibody solutions (stabilized by the non-gelling vegetable gelatin lambda-carrageenan), convenient incubation in jars and high reproducibility. This protocol was modified here according to the results obtained in the pilot studies (see above). Sections, stored at –20°C, were air-dried for 30 min at 37°C and immersed for antigen demasking into 0.01 M sodium citrate solution (pH 9.0, adjusted with 0.01 M NaOH) preheated to 80°C in a waterbath for 30 min (Jiao *et al.*, 1999). Following cooling of the slides to room temperature, blocking of non-specific binding sites was performed using phosphate-buffered saline (PBS, pH 7.3) containing 0.2% v/v Triton X-100, 0.02% w/v sodium azide and 5% v/v normal goat serum for 1 h at RT. Incubation with the primary antibody, diluted in PBS containing 0.5% w/v lambda-carrageenan and 0.02% w/v sodium azide, was carried out for 3 days at 4°C. After wash in PBS (3 × 15 min at RT) the appropriate secondary antibody diluted 1:200 in PBS–carrageenan solution (see above) was applied for 2 h at RT. Goat anti-rabbit or goat anti-mouse IgG conjugated with Cy3 (Jackson ImmunoResearch Laboratories, Dianova, Hamburg, Germany) was used for PV, CR, CB, NeuN, CNPase, S-100 and Iba1. Goat anti-rabbit IgG–Alexa Fluor® 555 (Molecular Probes, Leiden, The Netherlands) was applied for GAD and TNC. After a subsequent wash in PBS, cell nuclei were stained for 10 min at RT with *bis*-benzimide solution (Hoechst 33258 dye, 5 μg/ml in PBS, Sigma). Finally, the sections were washed again, mounted in anti-fading medium (Fluoromount G, Southern Biotechnology Associates, Biozol, Eching, Germany) and stored in the dark at 4°C.

WFA staining was performed according to the same protocol using Cy3-streptavidin (1:200 in PBS, Jackson ImmunoResearch). Antigen retrieval also significantly improved the quality of this staining based on the lectin affinities to sugar moieties. For double labelling, WFA and PV antibody solution were mixed at optimal dilutions. Visualization was made with streptavidin–Alexa Fluor® 488 (Molecular Probes) and anti-mouse IgG–Cy3. Double immunostaining for NeuN and S-100 was performed by mixing the primary antibodies at optimal dilutions and using a Cy3-conjugated anti-mouse and a Cy2-labelled anti-rabbit secondary antibody preabsorbed with rabbit and mouse serum proteins respectively (multiple-labelling grade antibodies, Jackson ImmunoResearch). For a given antigen, all sections were stained in the same solution kept in screw-capped staining plastic jars (capacity 35 ml, 10 slides, Roth). Specificity of staining was tested by omitting the first antibody or replacing it by variable concentrations of normal serum or IgG. In both mutant and wild-type animals the morphology of the immunofluorescent cells appeared to be characteristic of the cell type expected to be labelled (Fig. 1*B–G*, Fig. 2*A,B*).

Stereological Analysis

Numerical densities were estimated using the optical disector method (Gundersen, 1986). Counting was performed on an Axioskop microscope (Zeiss, Oberkochen, Germany) equipped with a motorized stage and Neurolucida software-controlled computer system (MicroBrightField Europe, Magdeburg, Germany). Four spaced-serial sections 250 μm apart, cut at distances between 7 and 8 mm rostrally from the caudal pole of the cerebellum (where collection of section began, see above), were examined per staining and animal. The agranular motor and the granular sensory areas (M and S respectively in Fig. 1*A*) were identified at low magnification by viewing the nuclear staining (Plan-Neofluar®
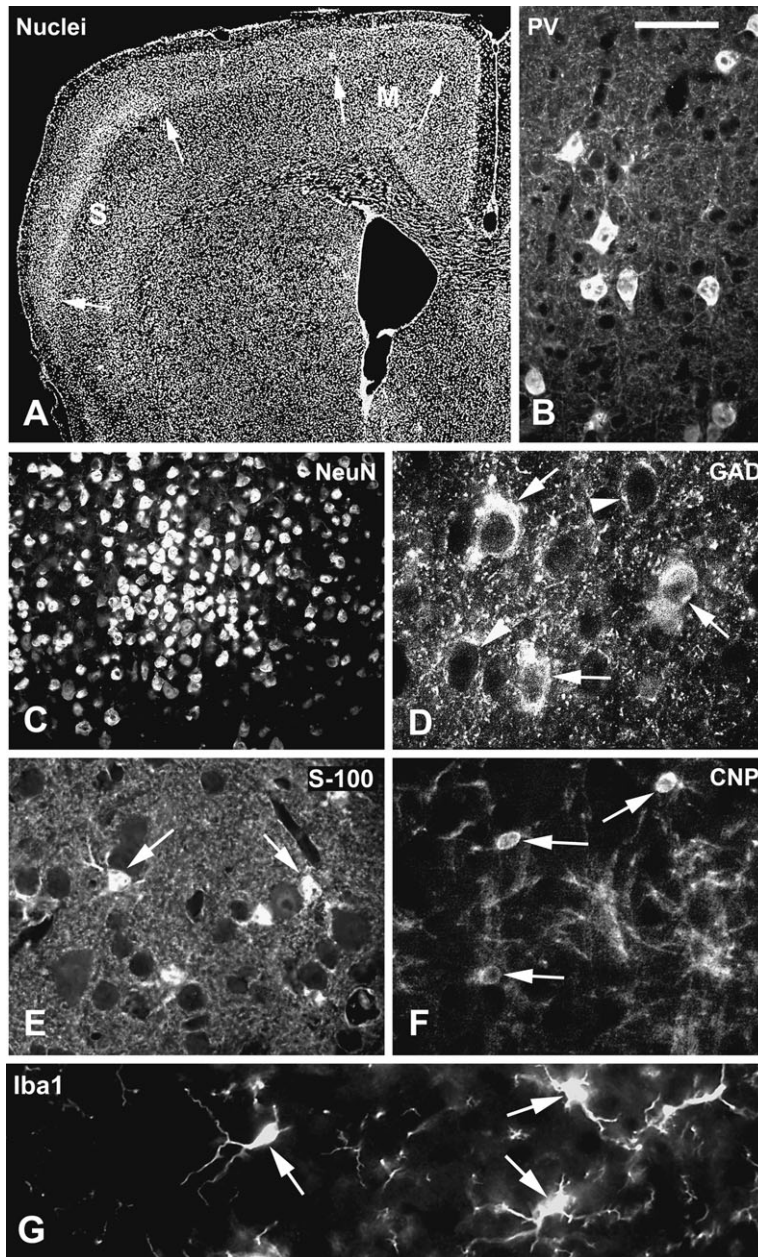
Figure 1. Nuclear staining (*A*) and examples of immunohistochemical stainings (*B–F*) in sections of TNC−/− (*A*, *B*, *E*, *G*) and TNC+/+ (*C*, *D*, *F*) animals. (*A*) A low-power view of the nuclear staining shows the delineation of the motor (M) and sensory (S) cortex areas by the different nuclear densities in layer IV (arrows). (*B*) PV+ neurons in layer IV of the sensory cortex. (*C*) Densely clustered cell profiles in the centre of the picture are NeuN+ neurons in a barrel of the sensory cortex. It should be noted that NeuN is detectable not only in the nucleus but also in the cell body (see also Wolf *et al.*, 1996); this, however, is not discernible here without nuclear counterstain overlay. (*D*) GAD+ cells (arrows), labelling in the neuropil and around GAD-negative cells (arrowheads) are seen in layer V of the motor cortex. (*E*) S-100+ astrocyte cell bodies (arrows) and astrocyte processes in the neuropil in layer IV of the sensory cortex. (*F*) CNPase+ cell bodies (arrows) and processes in layer 2 of the sensory cortex. (*G*) Iba1+ cells (arrows) located in a barrel field of the somatosensory cortex. Scale bar in (*B*) indicates 700, 50, 70, 20, 30, 30 and 11 µm for (*A*)–(*G*), respectively.

10×/0.3 objective). The contours of the sensory or motor cortical segments, excluding layer I, were outlined with the cursor. Nuclei of immunolabelled cells were counted within systematically randomly spaced optical disectors throughout the delineated area. The parameters for the quantitative analysis were: guard space depth 2 µm, base and height of the disector 3600 µm^2 and 10 µm respectively, distance between the optical disectors 60 µm for the motor and 90 µm for the sensory cortex, objective 40× Plan-Neofluar® 40×/0.75. A disector depth of 10 µm appeared appropriate since antibody penetration was sufficient to enable clear recognition of stained objects to a depth of at least 15 µm. At least one motor and one sensory cortex field in the left or right hemisphere was evaluated per section. For both genotypes, the

number of samples from the left and the right hemisphere was roughly equal. All counts were performed on coded preparations by one observer. Values for all morphological parameters are expressed as means ± SD.

We also evaluated section thickness using the nuclear staining. Nuclear 'caps' (cut tiny portions of the nuclei) clearly delineated the two surfaces of the sections. The mean section thickness was 24 ± 1.5 µm (20 sections from 10 brains). This value differed little (4%) from the intended sectional thickness (25 µm). Assuming precision of the cutting instrument, this finding indicates little tissue shrinkage in the z-axis. We did not perform corrections of the density estimates for shrinkage or distortion.
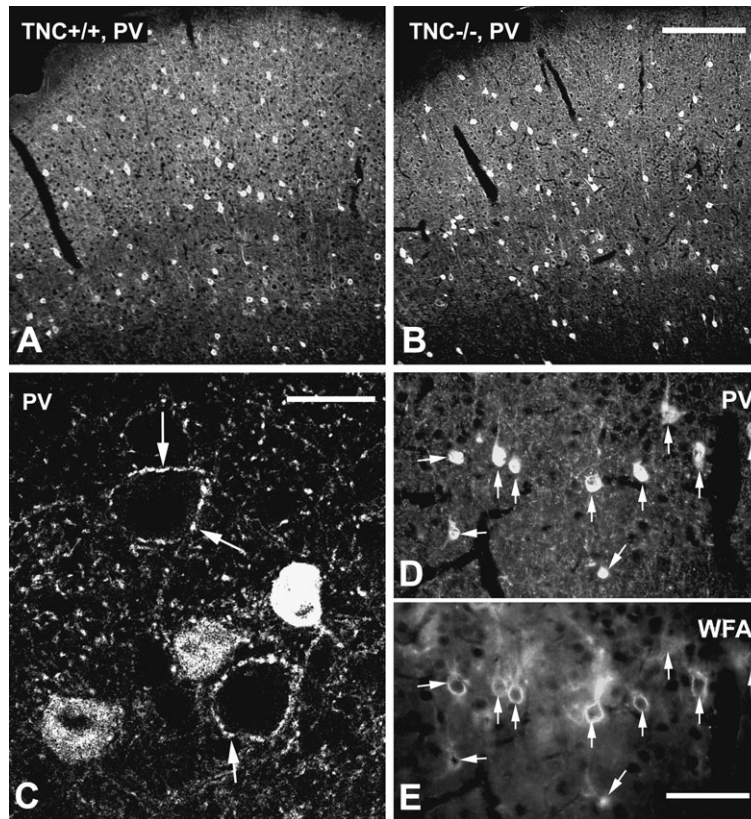
Figure 2. Parvalbumin (*A–D*) and lectin (*E*) staining in the sensory cortex of wild-type (*A*) and mutant (*B–E*) animals. (*A, B*) Low-magnification views show the distribution of PV$^+$ neurons. (*C*) A confocal image (1 µm thick optical slice) shows PV$^-$ cell body profiles surrounded by perisomatic structures (arrows). (*D, E*) Double labelling of PV$^+$ (*D*) and WFA$^+$ (*E*) cells in the visual field shows co-localization (arrows). Scale bars indicate 200 µm (*A, B*), 20 µm (*C*) and 50 µm (*D, E*).

The morphological analyses produced a data set on numerical densities of all cell nuclei and of seven immunohistochemically defined cell types in the motor and sensory cortices of wild-type mice (see Results). Evaluation of these results with regard to previous work is impossible because stereological data on mouse cortex could not be found in the literature. The only exception are three reports on numerical densities of neurons estimated using routinely stained histological preparations (Schüz and Palm, 1989; Miki *et al.*, 1994; Abreu-Villaca *et al.*, 2002). Our estimates of total neuronal density based on NeuN staining (96 and 111 × 10^3 mm^{-3} in the motor and sensory cortices respectively) are within the range reported for different cortical areas (66–144 × 10^3 mm^{-3}).

Analyses of Spatial Cell Distribution and Cortical Thickness

Analysis of first nearest neighbour distances and cell profile counts were performed for PV$^+$ neurons using the Neurolucida system and Plan-Neofluar 20×/0.5 objective (Zeiss). The motor or sensory cortical area was individually encircled and all profiles within the marked area were labelled by a symbol. Area and profile number were read from the Neurolucida screen. Mean nearest neighbour distances were calculated using Neuroexplorer software (MicroBrightField). Profile density was calculated by normalizing profile number to area. Four fields were measured per animal and cortical type.

Cortical thickness varied significantly within a single cortical segment (Fig. 1*A*). To estimate the average thickness we divided the area of the delineated field by the length of its boundary facing the meningeal surface.

Quantification of Inhibitory (PV$^+$) Perisomatic Axonal Structures

We estimated numbers of PV$^+$ structures surrounding the cell bodies of presumptive pyramidal cells in layer V. Stacks of images of 1 µm thickness were obtained on a LSM 510 confocal microscope (Zeiss)

using a 40× oil immersion objective and the highest digital resolution (2048 × 2048 pixels) available. One image per cell at the level of the largest cell body cross-sectional area was used for measurement. The number of individually discernible structures was counted and normalized to the perimeter of the cell measured using Image Tool 2.0 software (University of Texas Health Science Center, San Antonio, Texas; Fig. 2*C*).

Golgi Impregnations and Quantitative Analyses of Pyramidal Neurons

Under deep anaesthesia with Narcoren®, the animals were transcardially perfused with physiological saline followed by 10% formaldehyde in physiological saline and thereafter kept for 1 week at RT. After dissection of the brains, the tissue was processed according to the modified Golgi–Kopsch staining procedure (chromation in 3.6% w/v potassium dichromate solution followed by impregnation in 0.75% w/v silver nitrate solution, 5 days at RT each). Two additional cycles of chromation and impregnation (4 days each) were performed. Thereafter, 100 µm sagittal sections were cut on a Vibratome (VT1000S, Leica). The sections were dehydrated and coverslipped with DePeX (Fluka, Seelze, Germany).

The degree of linearity of apical pyramidal cell dendrites in layer V of the somatosensory and the motor cortices was evaluated according to Demyanenko *et al.* (1999) using the Neurolucida microscope system (20× objective). The dendrites were traced with the cursor and their curvilinear length divided by the length of a straight line connecting the ends of the measured dendritic segments (linearity index). At least 10 apical dendrites were measured per animal.

For estimation of spine density, pyramidal neurons (at least five per area and animal) were analyzed with the Neurolucida system (100× oil objective). Only dendrite segments oriented parallel to the surface of the section were selected for evaluation. Spines of different morphological appearance [stubby, mushroom and thin (Peters and Kaiserman-Abramof, 1970); Fig. 8*A*–*C*] were counted and normalized to dendrite

length. Analyses of dendrites was performed by one observer on coded preparations.

Epicranially Recorded Sensory Evoked Potentials (SEPs)

Epicranial SEP recordings were performed as described previously (Troncoso *et al.*, 2000). Briefly, the mouse head was placed in a stereotaxic frame under sodium pentobarbital anaesthesia (60 mg/kg i.p.) and loss of eyeblink and withdrawal reflexes was monitored to assess anaesthesia depth. Body temperature was maintained at ~37°C. A series of 10 electromechanical stimuli driven by a computer-controlled signal were applied unilaterally at 10 min intervals to all whiskers at a distance of 10 mm from the face with a vertical excursion of 300 μm in the dorsoventral direction and an interstimulus interval of 3 s. Evoked potentials were recorded by an array of three stainless steel macro-electrodes (0.45 mm in external diameter and 2 cm length), placed in tight contact with the skull contralateral to the stimulation side at the following coordinate points relative to bregma: AP –1/L 2.5, AP –2/L 3.0 and AP –3/L 3.5 (distance in mm). Signals were amplified (×10 000) and filtered (high pass 4 Hz, low pass 300 Hz), then hooked up and digitally converted (16 bits, 2 kHz with triggered scan) and stored for *post hoc* analysis. At the end of the recordings, the skull was carefully cleaned and the skin closed with surgical suture.

Results represent the mean of three averaged responses recorded at 10 min intervals. Peak positive and negative values between 10 and 30 ms post-stimulus were analyzed. Variables measured and evaluated were peak-to-peak amplitude, inter-peak slope and positive peak latency of the SEP responses (see Fig. 9*B*). The values are expressed as means ± SEM.

Photographic Documentation and Statistical Analysis

Photographic documentation was made on an Axiophot 2 microscope equipped with a digital camera AxioCam HRC and AxioVision software (Zeiss) at highest resolution (2300 × 2030 pixels, RGB). The images were additionally processed using Adobe Photoshop 6.0 software (Adobe Systems Inc., San Jose, CA).

Group mean values were compared using SigmaStat 2.0 software (SPSS, Chicago, IL). A parametric (*t*-test, two-sided) or a non-parametric test (Wilcoxon–Mann–Whitney *U*-test) for independent groups was chosen in accordance with the results of tests for equal variance and normal distribution. By two or more measurements per parameter and animal, the mean was used as a representative value. Thus, for all comparisons the degree of freedom was determined by the number of animals. The accepted level of significance was 5%.

Results

Morphological Analyses

Examinations of sections stained with *bis*-benzimide revealed typical six-layer organization of the somatosensory and motor cortices in both wild-type (TNC+/+) and TNC deficient (TNC–/–) animals without evidence for any apparent genotype-related abnormalities. This is in agreement with previous observations of normal histological appearance of the neocortex, in particular the barrel cortex in TNC deficient animals (Steindler *et al.*, 1995).

In TNC+/+ animals, mean values of the variables studied in the motor cortex generally differed little from those in the sensory cortex (Figs 3, 4, 6, compare black bars in *A* and *B*) with two exceptions: the numerical densities of neurons and total cell density were higher in the sensory versus the motor cortex (111 ± 6.6 versus 96 ± 10 and 270 ± 7.4 versus $223 \pm 14 \times 10^3$ cells/mm^3, +16% and +20% respectively, $P < 0.05$ for both, *t*-test, compare first and second black bars from left in Fig. 3*A* with the corresponding ones in Fig. 3*B*). Since the differences observed between mutant and wild-type animals had the same magnitude in both cortical areas, the results will be described jointly.
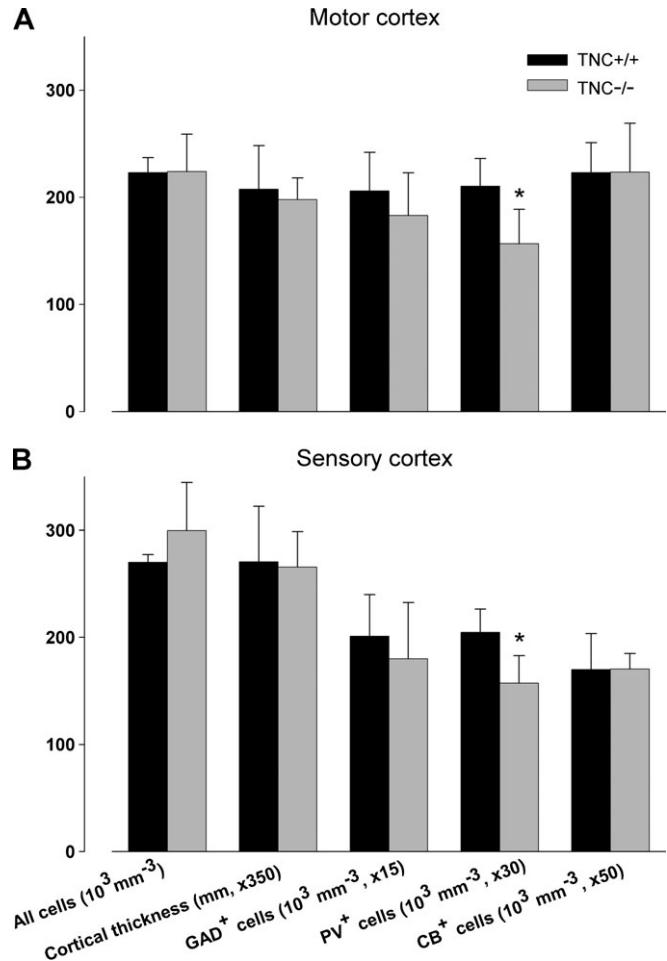

Figure 3. Total cell density, cortical thickness and numerical densities of inhibitory neurons (GAD$^+$, PV$^+$ and CB$^+$) in the motor (*A*) and sensory (*B*) cortices. Shown are mean values + SD for TNC+/+ ($n = 5$, black bars) and TNC–/– ($n = 5$, grey bars) mice. Asterisks indicate statistically significant differences between the groups ($P < 0.05$, *t*-test). Multiplication factors are used to adapt some values to the scaling.

Observations on Inhibitory Interneurons

The numerical density of GAD$^+$ (GABAergic) cells in TNC–/– mice was not statistically different from that in TNC+/+ animals (Fig. 3*A*,*B*, third bar pairs from left). Also, no differences between the genotypes were found for two subpopulations of GABAergic cells: calbindin (CB$^+$) interneurons (Fig. 3*A*,*B*, last bar pairs on the right) and calretinin (CR$^+$) interneurons (1900 ± 470 versus 1790 ± 540 mm^{-3} and 1370 ± 540 versus 1280 ± 520 mm^{-3}, mean ± SD, in the motor and sensory cortices of TNC+/+ and TNC–/– animals respectively). However, the numerical density of par-valbumin (PV$^+$) cells, the main subpopulation of the GABAergic neurons in the cortex, was significantly lower (25%) in the mutant animals (Fig. 3*A*,*B*, fourth bar pairs from left). Comparison of the density of PV$^+$ and GAD$^+$ cells shows that the former comprise about one-half of the GABAergic population in TNC+/+ mice (Fig. 3, note the similar height of the black bars and the 2-fold difference in the multiplication factors indicated below the bars). Thus, a 25% reduction in the number of PV$^+$ cells should result in a 13% smaller GAD$^+$ population. The difference between the mean values of GAD$^+$ neurons in the two genotype groups was 11%.

To obtain a reference value for the densities of immunohisto-chemically identified cells, we analysed the density of all
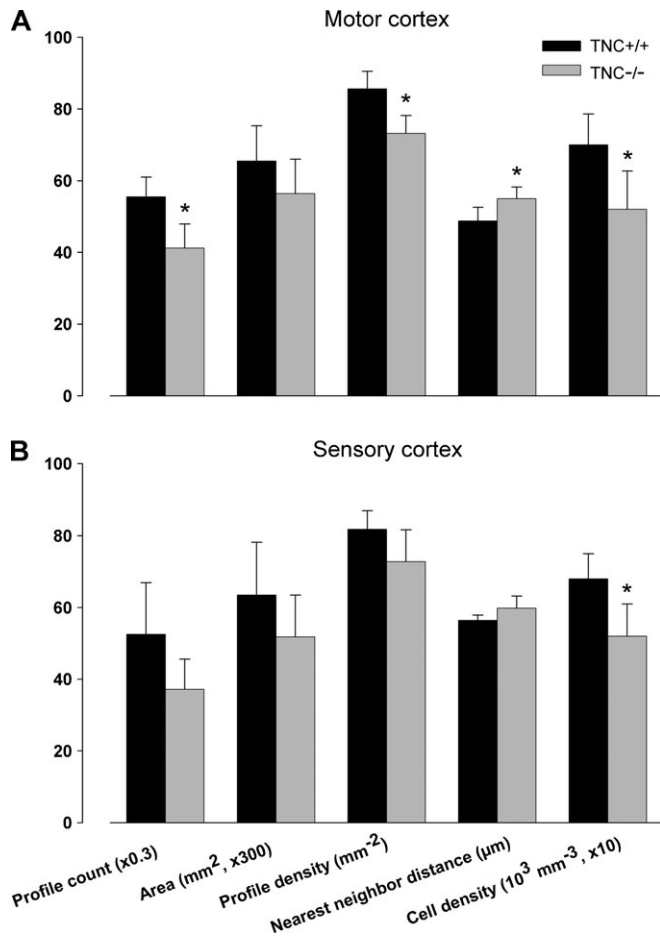
Figure 4. Results of the two-dimensional analysis of PV+ neurons. Shown are mean values + SD for TNC+/+ (black bars) and TNC−/− (grey bars) mice (n = 5 per genotype). *P < 0.05, t-test. Multiplication factors are used to adapt some values to the scaling.

cortical cells identified by nuclear staining. These values were higher in the sensory as compared the motor cortex in both groups but there were no differences between the genotypes (see above and Fig. 3A,B, first bar pairs from left). Thus, the density of PV+ neurons in the mutant mice was also significantly smaller (25–30%) when related to the total cell number. An estimate of cortical thickness (layers II–VI) was also made and no difference was found (Fig. 3, second bar pairs from left). This implies that the number of PV+ cells under a unit of cortical surface is significantly smaller in the mutant animals (–25%).

We also performed a nearest neighbour distance analysis to obtain insight into the spatial distribution of PV+ neurons. The average distance between PV+ cell profiles in the motor cortex was slightly but significantly higher in the mutant animals (+13%, P < 0.05, t-test, Fig. 4A, fourth bar pair from left). A similar tendency was found in the sensory cortex (+6%, P < 0.08, t-test, Fig. 4B). These findings correlate with the estimates of cell density (Fig. 4, last bar pairs on the right-hand side). Increased intercellular distances may be interpreted as an indication of loss of cells within a similar reference area. The distance analysis also produced data on cell profile numbers and densities. There was a good correspondence between the profile estimates and the values for the numerical densities (Fig. 4, compare first and third bar pairs from left with the last on the right hand side).

To estimate the inhibitory input to pyramidal cortical neurons in layer V we quantified PV+ structures appearing to be aligned along cell surfaces (Fig. 2C). The number of perisomatic structures (normalized to cell perimeter) in the motor cortex of TNC−/− mice was 15% smaller than in wild-type animals (33 ± 3.4 versus $28 \pm 4.5 \times 10^2$ μm^{-1}, 29 and 15 cells from three and two animals studied respectively, $P < 0.05$, t-test). A similar difference (18%) was found in the sensory cortex (32 ± 3.8 versus $26 \pm 5.0 \times 10^2$ μm^{-1}, 22 and 20 cells from three and two animals studied respectively, p < 0.05, t test). Thus, the density of PV+ cells correlated with the number of PV+ perisomatic axonal structures.

Differences in numbers of immunocytochemically identified cells can simply reflect loss of immunoreactivity. To investigate this possibility, we compared PV immunolabelling with WFA lectin staining of perineuronal nets known to surround PV+ cells. This was done by double labelling of sections from two animals of each genotype (Fig. 2D,E). Comparison of the staining pattern of individual cells (~200 per animal) revealed no differences between the two genotypes. In the sensory cortex of individual animals, 94–96% of all stained cells (positive for PV or WFA, or both) were PV+WFA+. Only small percentages of the two other possible staining patterns were observed (1–2% WFA+PV−, 3–4% WFA−PV+). These findings allow the conclusion that lower densities of PV+ cells in the mutant animals did not result from loss of PV immunoreactivity.

We analysed the expression of TNC in the mouse cortex in relation to its possible influence on the structure of perineuronal nets surrounding PV+ cells. Using a well-characterized polyclonal antibody (KAF 9-2), we were unable to detect TNC in the cortex in fixed cryostat sections of TNC+/+ and TNC−/− animals (not shown). However, in sections through the thalamus of wild-type, but not mutant mice, intensely labelled cells were found, indicating that TNC is not present in high amounts in the adult cortex. On fresh-frozen tissue sections from two C57BL/6J mice an interesting staining pattern was observed. In all parts of the sensory cortex diffuse labelling of layer Va was present (Fig. 5A). In the dysgranular zone of the sensory cortex also layers I–IV were stained (Fig. 5A). Immunolabelling in the motor cortex was most pronounced in layers II–III (not shown). These findings are in agreement with recent results of Kusakabe et al. (2001) which demonstrate that TNC is expressed, both at mRNA and protein level, in the adult neocortex of the mouse. Staining around blood vessels was seen in all cortical layers and areas (Fig. 5A). Comparison of TNC and WFA staining patterns in serial sections revealed that the overall TNC expression was low in areas containing numerous WFA+ neurons, such as those in layer IV of the sensory cortex (Fig. 5A,B). These observations indicate that TNC is not a major component of the perineuronal nets in the adult mouse cortex. Also, the appearance of perineuronal nets in TNC−/− mice was normal (Fig. 5C,D). In contrast, aberrations in the structure of perineuronal nets have been observed in mice deficient for tenascin-R, a known major protein component of the extracellular matrix surrounding PV+ interneurons (Weber et al., 1999).

Densities of Neurons and Glial Cells

Mean densities of oligodendrocytes (CNPase+) were similar in the two groups (Fig. 6, third bar pairs from the left). Also, no differences between the two animal groups were found in the density of microglial cells (Iba1+, 8.0 ± 0.8 versus 8.0 ± 1.5 and 7.4 ± 0.9 versus $7.7 \pm 1.1 \times 10^3$ mm^{-3} in the motor and
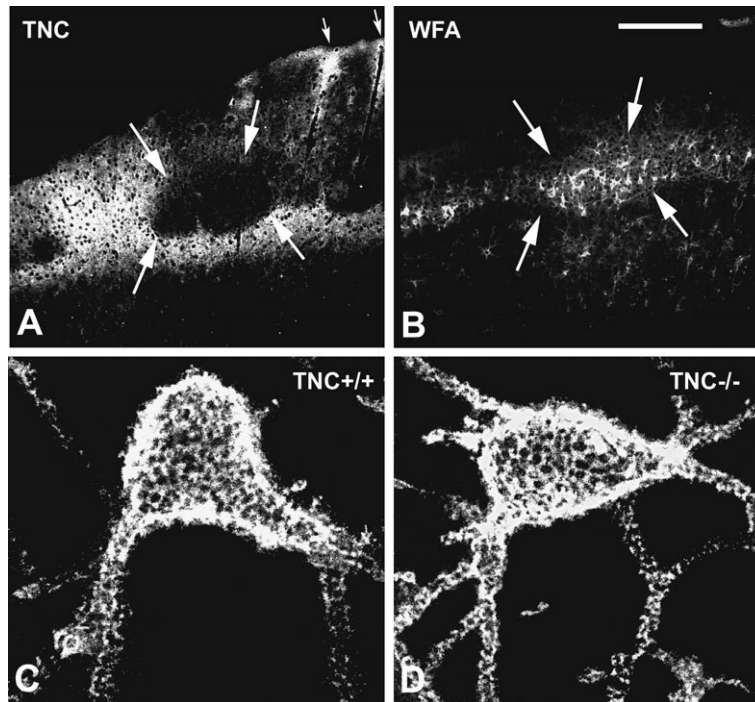
Figure 5. TNC and perineuronal nets. (*A, B*) TNC (*A*) and perineuronal nets visualized by WFA (*B*) in serial sections of the sensory cortex of a C57BL/6J mouse. Layer IV contains numerous WFA-labelled cells (area enclosed by arrows in *B*) but little TNC (*A*). The labelling of layers I–III to the left of the arrows in (*A*) is confined to the dysgranular cortex identified by nuclear staining (not shown). Small arrows in (*A*) point to blood vessels surrounded by TNC immunofluorescence. (*C, D*) WFA labelling reveals normal appearance of perineuronal nets in a TNC−/− (*C*) as compared to a TNC+/+ (*D*) animal. Stacks of superimposed confocal images (20 × 1 μm). Scale bar in (*B*) indicates 200 μm for (*A, B*) and 10 μm for (*C, D*).

somatosensory cortex of TNC+/+ versus TNC−/− animals respectively, not significant, *t*-test). In view of this, and the findings that, on the one hand, PV$^+$ cell density is lower and, on the other, that total cell number in the mutants does not differ from control it was rather unexpected to find out that the numerical densities of all neurons (NeuN$^+$) and astrocytes (S-100$^+$) were significantly higher in the mutant animals (24% and 40–54% respectively, see Fig. 6, first two bar pairs from the left).

In previous studies labelling of neurons by S-100 antibodies have been observed (Rickmann and Wolff, 1995b; Yang *et al.*, 1995; Ogata and Kosaka, 2002). We performed double immunostainings to estimate the degree of overlap of the S-100 and NeuN labelling, especially with a view to the increased numerical densities of both neurons and astrocytes in the TNC−/− animals. In sections of two animals from each genotype we found no cells labelled for both S-100 and NeuN. From a total number of 947 randomly selected labelled cells observed in the motor and sensory cortices of TNC+/+ animals (about equal numbers examined in the two cortical areas), 856 cells were NeuN$^+$S-100$^-$, 91 NeuN$^-$S-100$^+$ and 0 NeuN$^+$S-100$^+$. Similar results were obtained for TNC−/− animals (881 NeuN$^+$S-100$^-$, 107 NeuN$^-$S-100$^+$ and 0 NeuN$^+$S-100$^+$ out of 988 immuno-labelled cells examined). Therefore, we can exclude the possibility that co-labelling accounts for the higher densities of neurons and astrocytes in TNC−/− animals as compared to TNC+/+ mice.

Ratios between Cell Populations

In order to understand more comprehensively the aberrations in the mutant animals, we analyzed also the relative proportions of different cell types. Three ratios were significantly smaller in TNC−/− as compared to TNC+/+ animals: (i) oligodendrocytes to all neurons (−19%, Fig. 6, last bar pairs on the right hand side); (ii) inhibitory GABAergic interneurons to non-GABAergic (predominantly excitatory) neurons (−32%, Fig. 6, third bar pairs from left); and (iii) PV$^+$ interneurons to all neurons (4.7 ± 1.1% versus 8.0 ± 1.8% and 4.0 ± 0.7% versus 6.6 ± 1.1% in the motor and sensory cortices of mutant and wild-type mice respectively, 40% difference, *P* < 0.05 for both cortical areas, *t*-test). It is also worth mentioning that the ratio astrocytes to neurons, although not statistically significant, was >20% higher in the mutant animals (Fig. 6, compare the differences between the black and grey bars for NeuN, first from the left in the figure, with the control-versus-mutant differences in the numbers of S-100$^+$ cells, second bar pairs).

Dendrite Morphology and Spine Density

Golgi-impregnated pyramidal neurons in layer V of the motor and somatosensory cortices of TNC+/+ and TNC−/− animals appeared similar with respect to arborization, extralaminar extension and apical tufting. However, abnormally undulating apical dendrites were often seen in mutant animals (Fig. 7*B*) as opposed to the straight dendrites in wild-type mice (Fig. 7*A*). A similar difference between the phenotypes was observed for impregnated spiny stellate neurons (Fig. 7*C,D*). Quantitative analysis revealed a significantly increased linearity index in both the motor and somatosensory cortices of TNC−/− animals as compared to TNC+/+ animals (Fig. 7*E*).

No differences were found in the total spine densities on first- to third-order basal and apical dendrites of pyramidal neurons in the somatosensory cortex of mutant and wild-type animals (Fig. 8*D,E*). Densities of all spines in the motor cortex, as well as

densities of mushroom spines (Fig. 8B) and thin spines (Fig. 8C) in both cortical areas studied were similar in the two genotypes (data not shown). With regard to stubby spines (Fig. 8A), however, significant differences were found (Fig. 8F–I). In both motor and somatosensory cortices, this spine type was less frequent on first-order dendrites and more abundant on third-order basal and apical dendrites of TNC–/– animals as compared to TNC+/+ animals (Fig. 8F–I). The genotype-specific differences for second-order basal dendrites (higher numbers in the TNC–/– animals) were opposite to those observed for second-order apical dendrites (lower numbers in mutant mice, Fig. 8F and H versus Fig. 8G and I, respectively, bar pairs in the middle of the figures). These findings indicate an aberrant distribution of stubby spines among different parts of the dendritic tree in TNC–/– animals.

Somatosensory Evoked Potentials

To investigate the global activity of the somatomotor cortex, we applied multi-electrode epicranial recordings. Sensory evoked potentials (SEPs) were elicited by unilateral stimulation of all whiskers and recorded over the contralateral barrel and facial motor cortices with electrodes placed epicranially 2 mm caudal and 1 mm rostral from bregma respectively. Typical responses recorded over the barrel and motor cortices of a TNC+/+ and a TNC–/– mouse are shown in Figure 9A,B. The characteristic biphasic response is composed of a rapid positive peak (P1, mean delay of 13–14 ms) followed by a negative wave (N1, mean delay of 25–27 ms). The mean peak-to-peak amplitudes in TNC–/– mice were higher as compared to TNC+/+ animals (+60% and +120% in the barrel and motor cortices respectively, Fig. 9C). The values of SEP slopes, measured between the positive and the negative cortical responses (P and N in Fig. 9B), were also significantly higher in TNC–/– mice as compared to TNC+/+ animals (+80% and +120% in the barrel and motor cortices respectively, Fig. 9D). The peak latencies were similar in the two groups (21 ± 1.1 versus 20 ± 0.7 ms and 14 ± 0.7 versus 13 ± 0.7 ms in TNC+/+ versus TNC–/– animals in motor and sensory cortices respectively).

Discussion

The results of this study provide novel evidence for the functional importance of the ECM glycoprotein TNC for the development of the cerebral cortex. Studying adult TNC–/– and wild-type control mice, we observed physiological and structural features in the mutant mice that deviated significantly from those of control (TNC+/+) animals.

The numerical densities of three cell types, i.e. NeuN^{+} neurons, PV[+] interneurons and S-100[+] astrocytes, differ significantly in TNC–/– as compared to TNC+/+ animals. Importantly,
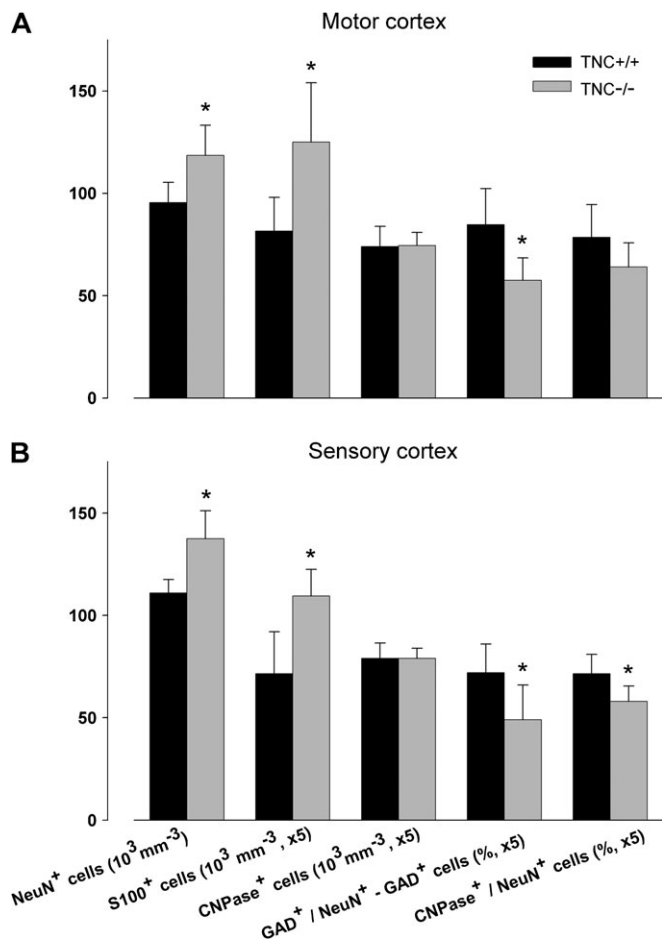

Figure 6. Densities of neurons (NeuN[+]), astrocytes (S-100[+]), oligodendrocytes (CNPase[+]) and ratios between populations. Shown are mean values + SD for TNC+/+ (black bars) and TNC–/– (grey bars) mice (n = 5 per genotype). Asterisks indicate statistically significant differences (P < 0.05, t-test). Multiplication factors are used to adapt some values to the scaling.

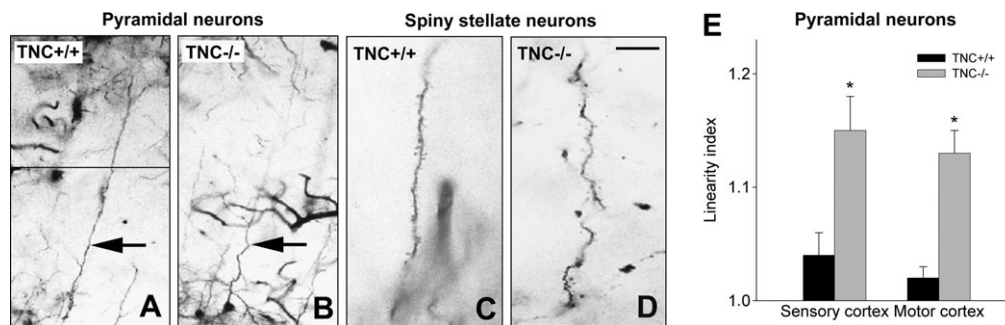**Figure 7.** Dendrite morphology of Golgi-impregnated pyramidal (A, B) and spiny stellate (C, D) neurons in the somatosensory cortex of TNC+/+ (A, C) and TNC–/– (B, D) animals. Apical dendrites of pyramidal neurons are marked with arrows (A, B). (E) Linearity index of pyramidal apical dendrites in the sensory and motor cortex of TNC+/+ (n = 7, black bars) and TNC–/– (n = 8, grey bars) animals. Shown are mean values + SD. Asterisks indicate statistically significant differences (P < 0.05, t-test). Scale bar in (D) indicates 40 μm for (A, B) and 10 μm for (C, D).
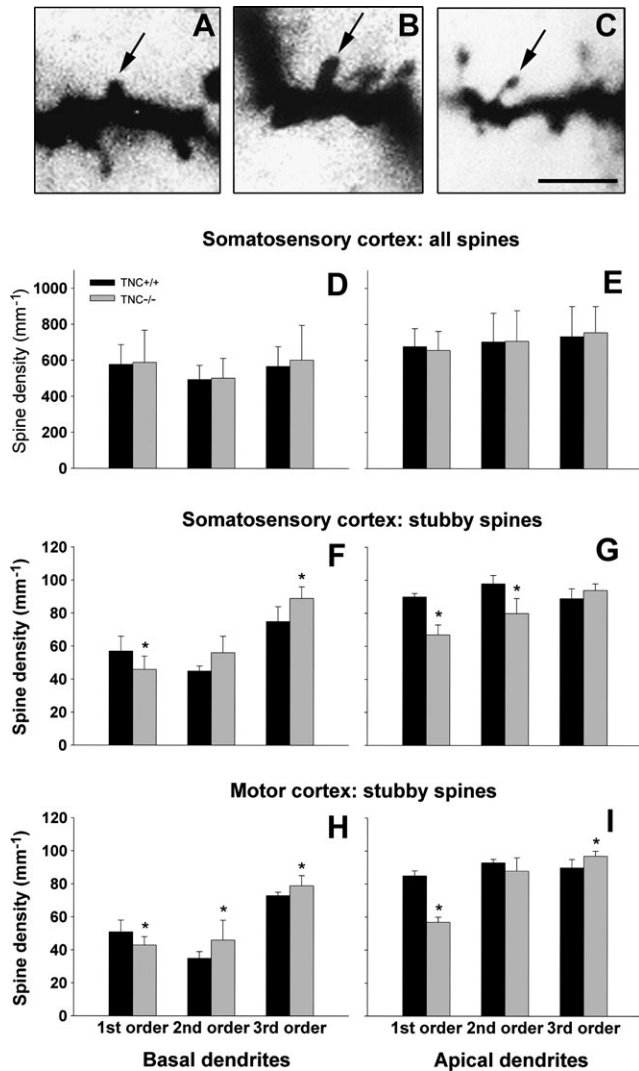
Figure 8. Examples of different spine types (stubby, *A*; mushroom, *B*; and thin spines, *C*) and densities of all spines in the somatosensory cortex (*D, E*) as well as of stubby spines (somatosensory cortex, *F, G*; motor cortex, *H, I*) on basal (*D, F, H*) and apical (*E, G, I*) dendrites of TNC+/+ ($n = 7$, black bars) and TNC−/− ($n = 8$, grey bars) animals. Shown are mean values + SD. Asterisks indicate statistically significant differences ($P < 0.05$, *t*-test). Scale bar in (*C*) indicates 5 µm for (*A–C*).

Figure 9. Epicranial SEP recordings. (*A, B*) Field potential changes recorded over the barrel (*A*) and motor (*B*) cortices contralateral to the stimulated whiskers in TNC+/+ and TNC−/− mice. Each trace is the average of three trials of 10 consecutive stimulations each. The biphasic primary responses are composed of a rapid positive peak (P in *B*) followed by a negative wave (N). (*C, D*) Mean amplitude (*C*) and slope values (*D*) + SEM for recordings over the barrel and motor cortices of TNC+/+ (black bars) and TNC−/− (grey bars, $n = 8$ for both genotype groups) animals. *$P < 0.05$, *t*-test.

these differences in densities reflect differences in absolute numbers of cells within a cortical column, i.e. volume underneath a unit cortical area, because the cortical thickness was similar in the two genotypes. The reasons for the aberrations can be sought in the developing cortex. A recent study by Garcion *et al.* (2004) has shown that TNC, which is highly expressed in the ventricular and subventricular zones, is an important regulator of neural stem cell behaviour during embryogenesis. One of the roles of TNC identified in this investigation is negative regulation of neurogenesis, indicated by the ability of TNC deficient neurospheres to produce a larger neuronal progeny *in vitro*. The present finding of an abnormally large neuronal population in the adult neocortex of the TNC−/− mouse is in good agreement with the *in vitro* observations. Furthermore, our results demonstrate inefficiency of compensatory mechanisms to correct the final neuronal numbers in the developing CNS. In fact, programmed cell death, a powerful mechanism controlling neuronal population size during devel-
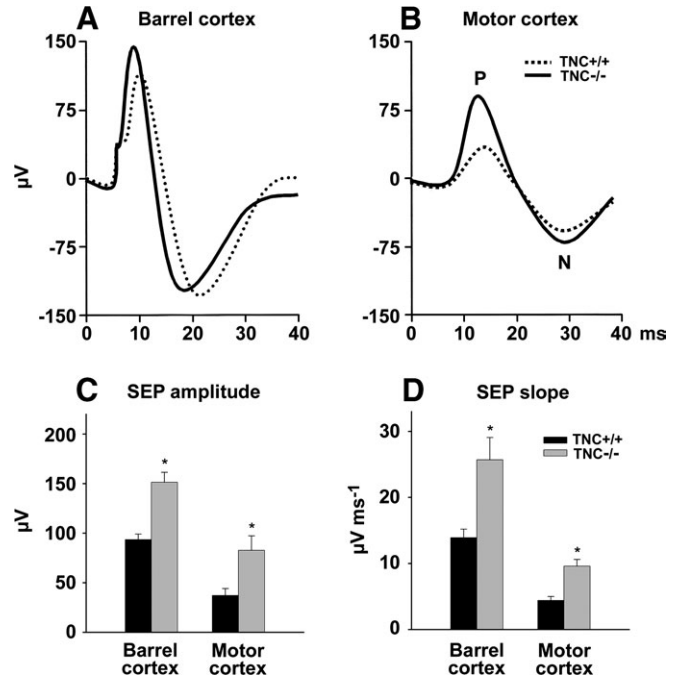
opment (Ferrer *et al.*, 1990, 1992; Naruse and Keino, 1995), appears to be reduced in the TNC-/- mouse. This is indicated by the finding of a lower frequency of apoptotic cells, positive as well as negative for oligodendrocyte markers, in the postnatal cortex of TNC deficient as compared to control wild-type mice (Garcion *et al.*, 2001).

The finding that the numbers of both neurons and astrocytes are increased in the cortex of mutant animals suggests that TNC might be crucial in regulating the properties and behaviour of one particular stem cell type, the radial glia cell, which is known to express TNC (Bartsch *et al.*, 1992; Stoykova *et al.*, 1997; Götz *et al.*, 1998). Radial glia cells generate both neurons and astrocytes in addition to providing scaffolding for neuronal migration (Doetsch, 2003; Rakic, 2003). The crucial role of radial glia cells during cortical development has been demonstrated in mice with mutations in the gene encoding the transcription factor *Pax6* (Stoykova *et al.*, 1996, 1997; Götz *et al.*, 1998). In this case, absence of functional gene product causes severe brain malformations due to loss of the neurogenic potential of radial glia and defective cell migration in areas where *Pax6* is normally expressed. And interestingly, in areas where defective *Pax6*-dependent neurogenesis occurs, e.g. the neocortex, radial cells do not express TNC. In the case of the TNC mutation, radial glia does indeed appear to be affected as indicated by the reduced number of RC2-positive cells in acutely dissociated brain tissue from embryos and newborn mice (Garcion *et al.*, 2004). This finding is in contrast to the observed increase in radial cells in Pax6 mutant mice (Götz *et al.*, 1998) and appears surprising in view of the larger neuronal progeny produced by TNC deficient stem cells both *in vitro* and *in vivo* (Garcion *et al.*, 2004; this study). The size of

a stem/ progenitor population, however, should not necessarily correlate with the number of differentiated daughter cells. In support of this notion is the evidence that, in contrast to the RC2-positive radial glia cells, the population of FGF2-responsive stem cells which are likely to differentiate into neurons is increased in association with the TNC deficiency (Garcion et al., 2004). Future research will have to identify exactly how TNC participates in the control of cortical development, both in terms of influences on different stem/ progenitor populations and expression of other regulatory factors.

Enhanced neurogenesis may explain the findings on total neuronal density and proportion of non-GABAergic neurons (NeuN[+] minus GAD^{+} cells) but not on GABAergic neurons. The latter were not increased in number as compared to wild-type animals and the PV[+] subpopulation was significantly smaller. With respect to this finding, one has to consider the fact that most inhibitory cells are generated in and migrate tangentially into the cortex from the medial ganglionic eminence, unlike excitatory neurons that follow a radial migratory route from the ventricular zone (Fairen et al., 1986; Xu et al., 2003). Regional differences in the specifications of neural stem cells such as, for example, Pax6 expression have been documented for the ventral telencephalon (ganglionic eminence) as compared to the dorsal telencephalon (ventricular zone) (Stoykova et al., 1997; Götz et al., 1998; Hack et al., 2004). Therefore, we can attribute the lack of hyperplastic effect in the TNC−/− mice on the tangentially migrating cell population, as opposed to the radially migrating neurons, to differential regulatory functions of TNC in the two brain regions, especially with regard to the generation of inhibitory neurons. Yet another possibility is that higher numbers of neurons are also generated in the ventral telencephalon. This notion is supported by the finding of enhanced neurogenesis in vitro of cells isolated from that region (Garcion et al., 2004). Therefore, it can be proposed that the tangential neuronal migration is impaired in the absence of TNC. Part of the tangentially migrating cells have to traverse, starting as early as day 16 in utero, a TNC-enriched environment located at the border between the lateral ganglionic eminence and the developing cortex (Fairen et al., 1986; Götz et al., 1997; Stoykova et al., 1997). If we assume a promoting function of TNC (see Faissner et al., 1994, for repulsive and growth-promoting properties of TNC), tangential migration might be disturbed in the mutant mouse.

The density of PV[+] interneurons appeared to be specifically reduced in TNC−/− as compared to wild-type animals. We could rule out that this was a result of loss of immunoreactivity or abnormalities of perineuronal nets. We can speculate that this deficiency results from migratory disturbances as suggested for the total GABAergic population. In addition, TNC deficiency may have a specific impact on the establishment of proper synaptic connections and cell type specification (see Xu et al., 2003, for origins and specification of cortical interneurons). Parvalbumin expression in a subpopulation of inhibitory neurons begins in the second postnatal week and is believed to be related to physiological maturation (Del Rio et al., 1994; Seo-Hiraiwa et al., 1995; Alcantara et al., 1996). The chemical specification of the PV subpopulation of GABAergic cortical neurons appears to be promoted by dopamine (Porter et al., 1999). Previous work has shown that tyrosine hydroxylase activity and mRNA levels are reduced in TNC deficient mice, suggesting lower dopamine levels (Fukamauchi et al., 1996). Therefore, the lower number of PV[+] interneurons may be a consequence of a maturational deficit during postnatal cortical development.

We have also to consider the abnormally high density of astrocytes in the cortex of the TNC deficient animals. Astrogliosis, i.e. hyperplasia and/or hypertrophy of astroglial cells, is commonly associated with CNS injury due to trauma, degenerative diseases, excitotoxicity or intoxications (Eng and Ghirnikar, 1994; Little and O'Callagha, 2001; Garzillo and Mello, 2002; Borges et al., 2003). Neurodegenerative causes involving an activated immune system can be ruled out in the case of TNC deficiency since density and appearance of Iba1^{+} microglial cells were normal. It is thus likely that we have identified a novel type of astrogliosis unrelated to tissue damage. The origins of this aberration may reside in the developing brain and be related to altered functions of the radial glia as supposed for neuronal cells. But it is also likely that the increase in the numerical density is due to altered cortical cell composition, function and/ or astrocyte responsiveness to stimuli under physiological conditions. Astrocytes form a dynamic and heterogeneous population in the normal postnatal brain which is in a constant bidirectional communication with and interdependence on neuronal populations (Fields and Stevens-Graham, 2002; Fellin and Carmignoto, 2004). Therefore, it is reasonable to assume that the increase in astrocyte numbers represents a compensatory growth to adapt the population to a larger neuronal density and possibly higher neuronal activity in the TNC−/− animals. Enhanced neuronal activity in the adult organism triggers and maintains higher numbers of supporting cells. Studies on epilepsy show that astrocytes may proliferate in cases of increased neuronal excitability without apparent excitotoxicity (Khurgel et al., 1995). Under epileptiform conditions, spontaneous oscillations in the intracellular free Ca^{2+} concentrations have been described in neocortical astrocytes which might represent a mechanism regulating cell activation and replication (Tashiro et al., 2002). Another interesting hypothesis is that higher astrocyte densities are related to abnormal synaptogenesis and maintenance of supra-numerous synaptic contacts, an idea related to emerging insights into the functions of astroglial cells (Slezak and Pfrieger, 2003). Finally, evidence exists indicating that TNC has an influence on astrocyte proliferation and morphology in a paracrine/autocrine fashion (Nishio et al., 2003). Qualitative analysis of astroglial reaction to brain injury has suggested an altered response in TNC deficient mice as compared to wild-type control animals (Steindler et al., 1995). Therefore, one can assume that the abnormal size of the astrocyte population in TNC−/− animals may be related to altered responsiveness to normal exogenous stimuli due to dysfunctional self-regulatory mechanisms. It is of great interest to test more extensively the abilities of astrocytes and neurons to react to and to withstand CNS injury in association with TNC deficiency (Steindler et al., 1995; see also Kusakabe et al., 2001, for enhanced death of neurons upon loss of TNC expression). In contrast to astrocytes, oligodendrocyte density in the cortex of TNC deficient mice was normal. Previous studies have shown two effects of TNC deficiency in the developing cortex: reduced oligodendrocyte precursor migration and lower levels of oligodendrocyte cell death (Garcion et al., 2001). Our results support the view that the mechanisms controlling oligodendrocyte cell numbers are sufficiently balanced in the cortex such that this population is normal in size.

The structural aberrations in the cortex of TNC−/− mice identified in this study were not only confined to cell densities.

Golgi staining revealed that pyramidal neurons have abnormally undulated apical dendrites in the mutant animals, suggesting a role of TNC in shaping dendrite morphology. Similar abnormality has been observed in the cortex of mice deficient for the cell adhesion molecule L1 (Demyanenko et al., 1999). These findings indicate that cell recognition molecules, in addition to other factors (Whitford et al., 2002), are essential for cortical dendrite development. In addition, we observed differentially altered densities of stubby spines on dendrites of different orders. With respect to this finding, it is important to note that parts of the dendritic trees which showed morphological aberrations are confined to the superficial part of layer V, where we documented some TNC protein expression in the adult wild-type cortex.

Previous investigations have demonstrated the impact of TNC on the physiological properties of neurons and synapses. Studies on TNC deficient mice have revealed impairment of the L-type Ca^{2+} channel-dependent forms of synaptic plasticity in the CA1 region of the hippocampus (Evers et al., 2002). A deficiency in hippocampus-dependent contextual memory has been found in TNC–/– animals (Strekalova et al., 2002). Intra-hippocampal application in vivo of a TNC fragment containing the fibronectin type-III repeats 6–8, which has growth cone repelling properties in vitro, leads to impairment of memory retention and reduced levels of long-term potentiation (Strekalova et al., 2002). Finally, it has been shown that TNC interacts with voltage-gated sodium channels (Srinivasan et al., 1998). To investigate functional parameters in the cortex of TNC animals, here we applied multielectrode epicranial recording of sensory evoked potentials. This approach has been successfully used to uncover functional alterations and deficits in mutant animals and after lesions (Meins et al., 2001; Troncoso et al., 2004). We found that the somatosensory responses in the barrel and motor cortices evoked upon whisker stimulation are robustly enhanced in TNC–/– as compared to TNC+/+ animals. The surface potentials recorded in the present study are thought to reflect the activation of apical dendrites of thousands of pyramidal cells sharing architectural and temporal coherence and generating post-synaptic activity. The synchronized activity of pyramidal cells depends on a delicate balance between excitatory and inhibitory neurotransmission that could be altered in TNC–/– animals, leading to increased somatosensory evoked potentials. Previous results show that basal levels of excitatory transmission as well as facilitation in the hippocampus of TNC–/– animals are normal (Evers et al., 2002). We can, therefore, speculate that inhibitory mechanisms in the cortex of TNC–/– animals are defective. This notion is concordant with the present morphological findings of lower numerical density of PV⁺ neurons, fewer PV⁺ structures around pyramidal cells in the mutant animals and reduced ratio of inhibitory to excitatory neurons. PV⁺ interneurons, coupled both chemically and electrically, form an inhibitory cortical network operating at high-frequency discharge rates and appear to be of major importance for basic cortical properties such as synchronization and oscillatory activities (Fukuda and Kosaka, 2000; Galarreta and Hestrin, 2002; Freund, 2003). Mice deficient for another member of the tenascin family, tenascin-R, have impaired inhibition and, similar to TNC–/– animals, enhanced cortical evoked potentials (Saghatelyan et al., 2001; Gurevicius et al., 2004). Interestingly, increased excitability in the tenascin-R mutant animals does not give rise to a more severe or accelerated epileptogenesis in the pilocarpine model of epilepsy (Brenneke et al., 2004). TNC–/– mice do not appear to be more susceptible than TNC+/+ animals to pilocarpine-induced seizures, either (A.A. Lie, personal communication).

In conclusion, we have identified aberrations in the cortex of TNC deficient mice suggesting cell-type specific effects on cell replication, migration, death, differentiation and connectivity during development. Future studies on the regulatory functions of TNC on stem and precursor cell populations and their progenies will definitely provide further insights into the mechanisms controlling normal development and functions of the CNS. Another exciting perspective will be the study of higher system levels of synaptic physiology in the TNC deficient cortex in order to understand the consequences for information processing in conjunction with a more refined time-scale analysis of cytological aberrations.

Notes

References

Abreu-Villaca Y, Silva WC, Manhaes AC, Schmidt SL (2002) The effect of corpus callosum agenesis on neocortical thickness and neuronal density of BALB/cCF mice. Brain Res Bull 58:411–416.

Alcantara S, de Lecea L, Del Rio JA, Ferrer I, Soriano E (1996) Transient colocalization of parvalbumin and calbindin D28k in the postnatal cerebral cortex: evidence for a phenotypic shift in developing nonpyramidal neurons. Eur J Neurosci 8:1329–1339.

Bartsch U (1996) The extracellular matrix molecule tenascin-C: expression in vivo and functional characterization in vitro. Prog Neurobiol 49:145–168.

Bartsch S, Bartsch U, Dorries U, Faissner A, Weller A, Ekblom P, Schachner M (1992) Expression of tenascin in the developing and adult cerebellar cortex. J Neurosci 12:736–749.

Bartsch U, Faissner A, Trotter J, Dorries U, Bartsch S, Mohajeri H, Schachner M (1994) Tenascin demarcates the boundary between the myelinated and nonmyelinated part of retinal ganglion cell axons in the developing and adult mouse. J Neurosci 14:4756–4768.

Borges K, Gearing M, McDermott DL, Smith AB, Almonte AG, Wainer BH, Dingledine R (2003) Neuronal and glial pathological changes during epileptogenesis in the mouse pilocarpine model. Exp Neurol 182:21–34.

Brenneke F, Bukalo O, Dityatev A, Lie AA (2004) Mice deficient for the extracellular matrix glycoprotein tenascin-r show physiological and structural hallmarks of increased hippocampal excitability, but no increased susceptibility to seizures in the pilocarpine model of epilepsy. Neuroscience 124:841–855.

Crossin KL, Hoffman S, Tan SS, Edelman GM (1989) Cytotactin and its proteoglycan ligand mark structural and functional boundaries in somatosensory cortex of the early postnatal mouse. Dev Biol 136:381–392.

Del Rio JA, de Lecea L, Ferrer I, Soriano E (1994) The development of parvalbumin-immunoreactivity in the neocortex of the mouse. Brain Res Dev Brain Res 81:247–259.

Demyanenko GP, Tsai AY, Maness PF (1999) Abnormalities in neuronal process extension, hippocampal development, and the ventricular system of L1 knockout mice. J Neurosci 19:4907–4920.

Doetsch F (2003) The glial identity of neural stem cells. Nat Neurosci 6:1127–1134.

Eng LF, Ghirnikar RS (1994) GFAP and astrogliosis. Brain Pathol 4:229–237.

Evers MR, Salmen B, Bukalo O, Rollenhagen A, Bosl MR, Morellini F, Bartsch U, Dityatev A, Schachner M (2002) Impairment of L-type Ca2+ channel-dependent forms of hippocampal synaptic plasticity in mice deficient in the extracellular matrix glycoprotein tenascin-C. J Neurosci 22:7177-7194.

Fairen A, Cobas A, Fonseca M (1986) Times of generation of glutamic acid decarboxylase immunoreactive neurons in mouse somatosensory cortex. J Comp Neurol 251:67-83.

Faissner A, Schachner M (1995) Tenascin and janusin: glial recognition molecules involved in neural development and regeneration. In: Neuroglia (Kettenmann H, Ransom BR, eds), pp. 422–426. New York: Oxford University Press.

Faissner A, Scholze A, Gotz B (1994) Tenascin glycoproteins in developing neural tissues: only decoration? Perspect Dev Neurobiol 2:53–66.

Fellin T, Carmignoto G (2004) Neuron-to-astrocyte signaling in the brain represents a distinct multifunctional unit. J Physiol 559:3-15.

Ferrer I, Bernet E, Soriano E, del Rio T, Fonseca M (1990) Naturally occurring cell death in the cerebral cortex of the rat and removal of dead cells by transitory phagocytes. Neuroscience 39:451-458.

Ferrer I, Soriano E, Del Rio JA, Alcantara S, Auladell C (1992) Cell death and removal in the cerebral cortex during development. Prog Neurobiol 39:1-43.

Fields RD, Stevens-Graham B (2002) New insights into neuron-glia communication. Science 298:556-562.

Forsberg E, Hirsch E, Frohlich L, Meyer M, Ekblom P, Aszodi A, Werner S, Fassler R (1996) Skin wounds and severed nerves heal normally in mice lacking tenascin-C. Proc Natl Acad Sci USA 93:6594-6599.

Freund TF (2003) Interneuron diversity series: rhythm and mood in perisomatic inhibition. Trends Neurosci 26:489-495.

Fukamauchi F, Mataga N, Wang YJ, Sato S, Youshiki A, Kusakabe M (1996) Abnormal behavior and neurotransmissions of tenascin gene knockout mouse. Biochem Biophys Res Commun 221:151-156.

Fukamauchi F, Mataga N, Wang YJ, Sato S, Yoshiki A, Kusakabe M (1997) Tyrosine hydroxylase activity and its mRNA level in dopaminergic neurons of tenascin gene knockout mouse. Biochem Biophys Res Commun 231:356-359.

Fukamauchi F, Aihara O, Kusakabe M (1998) Reduced mRNA expression of neuropeptide Y in the limbic system of tenascin gene disrupted mouse brain. Neuropeptides 32:265-268.

Fukuda T, Kosaka T (2000) The dual network of GABAergic interneurons linked by both chemical and electrical synapses: a possible infrastructure of the cerebral cortex. Neurosci Res 38:123-130.

Galarreta M, Hestrin S (2002) Electrical and chemical synapses among parvalbumin fast-spiking GABAergic interneurons in adult mouse neocortex. Proc Natl Acad Sci USA 99:12438-12443.

Garcion E, Faissner A, ffrench-Constant C (2001) Knockout mice reveal a contribution of the extracellular matrix molecule tenascin-C to neural precursor proliferation and migration. Development 128:2485-2496.

Garcion E, Halilagic A, Faissner A, ffrench-Constant C (2004) Generation of an environmental niche for neural stem cell development by the extracellular matrix molecule tenascin C. Development 131:3423-3432.

Garman RH (1990) Artifacts in routinely immersion fixed nervous tissue. Toxicol Pathol 18:149-153.

Garzillo CL, Mello LE (2002) Characterization of reactive astrocytes in the chronic phase of the pilocarpine model of epilepsy. Epilepsia 43(Suppl 5):107-9.

Götz M, Bolz J, Joester A, Faissner A (1997) Tenascin-C synthesis and influence on axonal growth during rat cortical development. Eur J Neurosci 9:496-506.

Götz M, Stoykova A, Gruss P (1998) Pax6 controls radial glia differentiation in the cerebral cortex. Neuron 21:1031-1044.

Gundersen HJ (1986) Stereology of arbitrary particles. A review of unbiased number and size estimators and the presentation of some new ones, in memory of William R. Thompson. J Microsc 143 (Pt 1):3-45.

Gurevicius K, Gureviciene I, Valjakka A, Schachner M, Tanila H (2004) Enhanced cortical and hippocampal neuronal excitability in mice deficient for the extracellular matrix glycoprotein tenascin-R. Mol Cell Neurosci (in press).

Hack MA, Sugimori M, Lundberg C, Nakafuku M, Gotz M (2004) Regionalization and fate specification in neurospheres: the role of Olig2 and Pax6. Mol Cell Neurosci 25:664-678.

Irintchev A, Salvini TF, Faissner A, Wernig A (1993) Differential expression of tenascin after denervation, damage or paralysis of mouse soleus muscle. J Neurocytol 22:955-965.

Irintchev A, Zeschnigk M, Starzinski-Powitz A, Wernig A (1994) Expression pattern of M-cadherin in normal, denervated, and regenerating mouse muscles. Dev Dyn 199:326-337.

Irintchev A, Rosenblatt JD, Cullen MJ, Zweyer M, Wernig A (1998) Ectopic skeletal muscles derived from myoblasts implanted under the skin. J Cell Sci 111:3287-3297.

Jiao Y, Sun Z, Lee T, Fusco FR, Kimble TD, Meade CA, Cuthbertson S, Reiner A (1999) A simple and sensitive antigen retrieval method for free-floating and slide-mounted tissue sections. J Neurosci Methods 93:149-162.

Jones PL, Jones FS (2000) Tenascin-C in development and disease: gene regulation and cell function. Matrix Biol 19:581-596.

Khurgel M, Switzer RC, III, Teskey GC, Spiller AE, Racine RJ, Ivy GO (1995) Activation of astrocytes during epileptogenesis in the absence of neuronal degeneration. Neurobiol Dis 2:23-35.

Kiernan BW, Garcion E, Ferguson J, Frost EE, Torres EM, Dunnett SB, Saga Y, Aizawa S, Faissner A, Kaur R, Franklin RJ, ffrench-Constant C (1999) Myelination and behaviour of tenascin-C null transgenic mice. Eur J Neurosci 11:3082-3092.

Kusakabe M, Mangiarini L, Laywell ED, Bates GP, Yoshiki A, Hiraiwa N, Inoue J, Steindler DA (2001) Loss of cortical and thalamic neuronal tenascin-C expression in a transgenic mouse expressing exon 1 of the human Huntington disease gene. J Comp Neurol 430:485-500.

Little AR, O'Callagha JP (2001) Astrogliosis in the adult and developing CNS: is there a role for proinflammatory cytokines? Neurotoxicology 22:607-618.

Meins M, Piosik P, Schaeren-Wiemers N, Franzoni S, Troncoso E, Kiss JZ, Brosamle C, Schwab ME, Molnar Z, Monard D (2001) Progressive neuronal and motor dysfunction in mice overexpressing the serine protease inhibitor protease nexin-1 in postmitotic neurons. J Neurosci 21:8830-8841.

Miki T, Fukui Y, Uemura N, Takeuchi Y (1994) Regional difference in the neurotoxicity of ochratoxin A on the developing cerebral cortex in mice. Brain Res Dev Brain Res 82:259-264.

Mitrovic N, Dorries U, Schachner M (1994) Expression of the extracellular matrix glycoprotein tenascin in the somatosensory cortex of the mouse during postnatal development: an immunocytochemical and in situ hybridization analysis. J Neurocytol 23:364-378.

Naruse I, Keino H (1995) Apoptosis in the developing CNS. Prog Neurobiol 47:135-155.

Nishio T, Kawaguchi S, Iseda T, Kawasaki T, Hase T (2003) Secretion of tenascin-C by cultured astrocytes: regulation of cell proliferation and process elongation. Brain Res 990:129-140.

Ogata K, Kosaka T (2002) Structural and quantitative analysis of astrocytes in the mouse hippocampus. Neuroscience 113:221-233.

Peters A, Kaiserman-Abramof IR (1970) The small pyramidal neuron of the rat cerebral cortex. The perikaryon, dendrites and spines. Am J Anat 127:321-355.

Porter LL, Rizzo E, Hornung JP (1999) Dopamine affects parvalbumin expression during cortical development in vitro. J Neurosci 19:8990-9003.

Rakic P (2003) Developmental and evolutionary adaptations of cortical radial glia. Cereb Cortex 13:541-549.

Rickmann M, Wolff JR (1995a) Modifications of S100-protein immunoreactivity in rat brain induced by tissue preparation. Histochem Cell Biol 103:135-145.

Rickmann M, Wolff JR (1995b) S100 protein expression in subpopulations of neurons of rat brain. Neuroscience 67:977-991.

Saga Y, Yagi T, Ikawa Y, Sakakura T, Aizawa S (1992) Mice develop normally without tenascin. Genes Dev 6:1821-1831.

Saghatelyan AK, Dityatev A, Schmidt S, Schuster T, Bartsch U, Schachner M (2001) Reduced perisomatic inhibition, increased excitatory transmission, and impaired long-term potentiation in mice deficient

for the extracellular matrix glycoprotein tenascin-R. Mol Cell Neurosci 17:226–240.

Schüz A, Palm G (1989) Density of neurons and synapses in the cerebral cortex of the mouse. J Comp Neurol 286:442–455.

Seo-Hiraiwa ML, Seto-Ohshima A, Kato K (1995) The surface evoked potential and parvalbumin-immunoreactivity in the somatosensory cortex of the developing rat. Dev Psychobiol 28:337–351.

Slezak M, Pfrieger FW (2003) New roles for astrocytes: regulation of CNS synaptogenesis. Trends Neurosci 26:531–535.

Sofroniew MV, Schrell U (1982) Long-term storage and regular repeated use of diluted antisera in glass staining jars for increased sensitivity, reproducibility, and convenience of single- and two-color light microscopic immunocytochemistry. J Histochem Cytochem 30: 504–511.

Srinivasan J, Schachner M, Catterall WA (1998) Interaction of voltage-gated sodium channels with the extracellular matrix molecules tenascin-C and tenascin-R. Proc Natl Acad Sci USA 95:15753–15757.

Steindler DA, Cooper NG, Faissner A, Schachner M (1989) Boundaries defined by adhesion molecules during development of the cerebral cortex: the J1/tenascin glycoprotein in the mouse somatosensory cortical barrel field. Dev Biol 131:243–260.

Steindler DA, O'Brien TF, Laywell E, Harrington K, Faissner A, Schachner M (1990) Boundaries during normal and abnormal brain development: *in vivo* and *in vitro* studies of glia and glycoconjugates. Exp Neurol 109:35–56.

Steindler DA, Settles D, Erickson HP, Laywell ED, Yoshiki A, Faissner A, Kusakabe M (1995) Tenascin knockout mice: barrels, boundary molecules, and glial scars. J Neurosci 15:1971–1983.

Stoykova A, Fritsch R, Walther C, Gruss P (1996) Forebrain patterning defects in Small eye mutant mice. Development 122:3453–3465.

Stoykova A, Gotz M, Gruss P, Price J (1997) Pax6-dependent regulation of adhesive patterning, R-cadherin expression and boundary formation in developing forebrain. Development 124:3765–3777.

Strekalova T, Sun M, Sibbe M, Evers M, Dityatev A, Gass P, Schachner M (2002) Fibronectin domains of extracellular matrix molecule tenascin-C modulate hippocampal learning and synaptic plasticity. Mol Cell Neurosci 21:173–187.

Tashiro A, Goldberg J, Yuste R (2002) Calcium oscillations in neocortical astrocytes under epileptiform conditions. J Neurobiol 50:45–55.

Troncoso E, Müller D, Czellar S, Kiss JZ (2000) Epicranial sensory evoked potential recordings for repeated assessment of cortical functions in mice. J Neurosci Methods 97:51–58.

Troncoso E, Muller D, Korodi K, Steimer T, Welker E, Kiss JZ (2004) Recovery of evoked potentials, metabolic activity and behavior in a mouse model of somatosensory cortex lesion: role of the neural cell adhesion molecule (NCAM). Cereb Cortex 14:332–341.

Vollmer G (1994) Expression of tenascin during carcinogenesis and involution of hormone-dependent tissues. Biochem Cell Biol 72:505–514.

Weber P, Bartsch U, Rasband MN, Czaniera R, Lang Y, Bluethmann H, Margolis RU, Levinson SR, Shrager P, Montag D, Schachner M (1999) Mice deficient for tenascin-R display alterations of the extracellular matrix and decreased axonal conduction velocities in the CNS. J Neurosci 19:4245–4262.

Whitford KL, Dijkhuizen P, Polleux F, Ghosh A (2002) Molecular control of cortical dendrite development. Annu Rev Neurosci 25:127–149.

Wolf HK, Buslei R, Schmidt-Kastner R, Schmidt-Kastner PK, Pietsch T, Wiestler OD, Bluhmke I (1996) NeuN: a useful neuronal marker for diagnostic histopathology. J Histochem Cytochem 44:1167–1171.

Xu Q, de la CE, Anderson SA (2003) Cortical interneuron fate determination: diverse sources for distinct subtypes? Cereb Cortex 13:670–676.

Yang Q, Hamberger A, Hyden H, Wang S, Stigbrand T, Haglid KG (1995) S-100 beta has a neuronal localisation in the rat hindbrain revealed by an antigen retrieval method. Brain Res 696:49–61.